

## An experimental study of the surface elevation probability distribution and statistics of wind-generated waves

By NORDEN E. HUANG AND STEVEN R. LONG

NASA Wallops Flight Center, Wallops Island, VA 23337

(Received 9 January 1979 and in revised form 5 December 1979)

Laboratory experiments were conducted to measure the surface elevation probability density function and associated statistical properties for a wind-generated wave field. The laboratory data together with some limited field data were compared. It is found that the skewness of the surface elevation distribution is proportional to the significant slope of the wave field,  $\xi$ , and all the laboratory and field data are best fitted by

$$K_3 = 8\pi\xi,$$

with  $\xi$  defined as  $(\overline{\zeta^2})^{1/2}/\lambda_0$ , where  $\zeta$  is the surface elevation, and  $\lambda_0$  is the wavelength of the energy-containing waves. The value of  $K_3$  under strong wind could reach unity. Even under these highly non-Gaussian conditions, the distribution can be approximated by a four-term Gram-Charlier expansion. The approximation does not converge uniformly, however. More terms will make the approximation worse.

---

### 1. Introduction

The surface elevation of any given point in the ocean is the resultant of many wave components. Dynamically, since the interactions between each component are weak (see, for example, Phillips 1977), their motions are largely regarded as independent. Consequently, under the central-limit theorem, the probability distribution of the surface elevation has been assumed to be Gaussian. The deviation from the Gaussian distribution due to the weakly nonlinear interaction has been shown theoretically by Phillips (1961) and Longuet-Higgins (1963) to be proportional to the wave slope. Up to now, the available data collected under very limited observational conditions by Kinsman (1960) can only support such a conclusion qualitatively.

With the increases in the application of active microwave remote sensing techniques, the importance of the knowledge of the detailed statistical characteristics also increases. The qualitative results of the past cannot satisfy the need of precise interpretation of the radar signals for present-day applications. The purpose of this paper is to present some field and laboratory data collected under a wide range of wind and wave conditions. The statistical properties of the surface elevation were processed for comparison with the theoretical results derived from Longuet-Higgins' (1963) theory. It was found that, even for the highly non-Gaussian cases, the distribution function proposed by Longuet-Higgins (1963) still gave good approximations.

### 2. The probability density function

According to the probability theory (see, for example, Cramer 1970), the characteristic function  $\phi(x)$  can be defined as the expected value of  $e^{ix\zeta}$ , i.e.

$$\phi(x) = \int_{-\infty}^{\infty} e^{ix\zeta} P(\zeta) d\zeta, \tag{2.1}$$

where  $P(\zeta)$  is the probability distribution function of any random variable,  $\zeta$ . Equation (2.1) also indicates  $\phi(x)$  as the Fourier transform of  $P(\zeta)$ . The inverse transformation will be

$$P(\zeta) = \frac{1}{2\pi} \int_{-\infty}^{\infty} \phi(x) e^{-ix\zeta} dx. \tag{2.2}$$

If the term  $e^{ix\zeta}$  is expanded in a power series, then (2.1) becomes

$$\begin{aligned} \phi(x) &= 1 + \mu'_1 \frac{(ix)}{1!} + \mu'_2 \frac{(ix)^2}{2!} + \dots + \mu'_r \frac{(ix)^r}{r!} + \dots \\ &= \exp \left\{ \lambda_1 \frac{(ix)}{1!} + \lambda_2 \frac{(ix)^2}{2!} + \dots + \lambda_r \frac{(ix)^r}{r!} + \dots \right\}, \end{aligned} \tag{2.3}$$

where  $\mu'_r$  and  $\lambda_r$  are the  $r$ th-order moment and cumulant respectively. If the moments (therefore, cumulants) exist for all orders, then the characteristic function can be expressed by moments. Consequently the probability distribution can also be determined by the moments uniquely. The relationships between the moments and cumulants of all orders are given implicitly by equation (2.3). If the moments taken with respect to the mean are indicated by  $\mu_r$ , then the first eight cumulants explicitly in terms of the moments (see, for example, Kendall & Stuart 1963, §§ 3.12–3.15) are

$$\left. \begin{aligned} \lambda_1 &= 0, \\ \lambda_2 &= \mu_2, \\ \lambda_3 &= \mu_3, \\ \lambda_4 &= \mu_4 - 3\mu_2^2, \\ \lambda_5 &= \mu_5 - 10\mu_3\mu_2, \\ \lambda_6 &= \mu_6 - 15\mu_4\mu_2 - 10\mu_3^2 + 30\mu_2^3, \\ \lambda_7 &= \mu_7 - 21\mu_5\mu_2 - 35\mu_4\mu_3 + 210\mu_3\mu_2^2, \\ \lambda_8 &= \mu_8 - 28\mu_6\mu_2 - 56\mu_5\mu_3 - 35\mu_4^2 + 420\mu_4\mu_2^2 + 560\mu_3^2\mu_2 - 630\mu_2^4. \end{aligned} \right\} \tag{2.4}$$

The values of moments and cumulants offer a quantitative means to measure whether a certain process is indeed Gaussian or not. For a Gaussian distribution,

$$\left. \begin{aligned} \mu_{2r} &= \frac{(2r)!}{2^r r!} \mu_2^r, \\ \mu_{2r+1} &= 0, \quad r \geq 1, \end{aligned} \right\} \tag{2.5}$$

for all  $r$ . And

$$\left. \begin{aligned} \lambda_2 &= \mu_2, \\ \lambda_r &= 0, \quad r > 2, \end{aligned} \right\} \tag{2.6}$$

for all  $r$ .

If a random process is nearly but not exactly Gaussian, the higher-order approximation can be expressed in terms of the moments and cumulants. For the gravity-wave surface elevation, both observations (Kinsman 1960) and theoretical analysis

(Longuet-Higgins 1963) suggested Edgeworth's form of the type A Gram-Charlier series (Kendall & Stuart 1963, § 6.18) would give the best approximation. The full Edgeworth's form up to the eighth term is given as

$$P(\zeta) = (2\pi K_2)^{-\frac{1}{2}} e^{-\frac{1}{2}t^2} \left[ 1 + \frac{1}{6}K_3 H_3 + \frac{1}{24}K_4 H_4 + \frac{1}{120}K_5 H_5 + \frac{K_6 + 10K_3^2}{720} H_6 + \frac{K_7 + 35K_4 K_3}{5040} H_7 + \frac{K_8 + 56K_5 K_3 + 35K_4^2}{40320} H_8 + \dots \right], \quad (2.7)$$

where  $t = \zeta/\mu^{\frac{1}{2}}$ ,  $K_r = \lambda_r/\lambda^{\frac{1}{2}r}$ , and  $H_r$  denotes the Hermite polynomial of degree  $r$ :

$$H_r = t^r - \frac{r(r-1)}{1!} \frac{t^{r-2}}{2} + \frac{r(r-1)(r-2)(r-3)}{2!} \frac{t^{r-4}}{2^2} - \dots \quad (2.8)$$

Edgeworth's form is derived by equating the probability distribution to the formal series expansion of derivatives of  $\alpha(t)$ , where

$$\alpha(t) = (2\pi)^{-\frac{1}{2}} e^{-\frac{1}{2}t^2}. \quad (2.9)$$

This form is very closely similar to the one given by Longuet-Higgins (1963),

$$P(\zeta) = (2\pi K_2)^{-\frac{1}{2}} e^{-\frac{1}{2}t^2} \left[ 1 + \frac{1}{6}K_3 H_3 + \left( \frac{1}{24}K_4 H_4 + \frac{1}{72}K_3^2 H_6 \right) + \dots \right]. \quad (2.10)$$

In fact, if one takes (2.7) up to the sixth term and sets  $K_r = 0$  for  $r \geq 5$ , one would get exactly (2.10). The justifications of not including  $K_r$  for  $r \geq 5$  are that higher-order cumulants might be unreliable owing to sampling fluctuations.

The objective of our study is to find out how close an approximation Edgeworth's expansion gives, and also to answer the question: Do the higher-order terms really improve the approximation?

### 3. Experimental procedures and data processing

The laboratory experiment was conducted at the Wallops Flight Center wind-wave-current research facilities. As shown in figure 1, the main test section is 18.29 m (60 ft) in length, 1.22 m (4 ft) in height, and 0.91 m (3 ft) in width. Its operational water depth is 0.76 m (2.5 ft) with 0.45 m (1.5 ft) remaining for air flow. Wind speed is variable between zero and 20 m s<sup>-1</sup>, while a water pump is present to generate variable and reversible current between zero and 0.5 m s<sup>-1</sup> in the water. The pump for current generation was not operated for this series of experiments.

This facility has a variety of data acquisition and processing capabilities. For this experiment, a capacitive-type wave height probe and the Datametries Pitot-tube system were used for data acquisition. The height probe was fixed at a fetch of 10.77 m, and the Pitot tube and Datametries type 572 transducer were placed just upwind, providing a vertical profile of the wind. All data processing was conducted in real time while the same data was recorded for future reference by an FM recorder.

For each wind speed, the following procedure was followed. After selecting a wind speed, the fan was left on for a half hour to insure a steady-state condition within the channel. This time was much longer than required for establishing a steady state in this tank. In fact, data collected after the fan had operated for ten minutes were identical to that taken after two hours. For special precaution, we allowed 30 min between changes of wind speeds, and 60 min at the beginning of each day.

To measure wind conditions, a Datametries electronic manometer (Pitot tube)

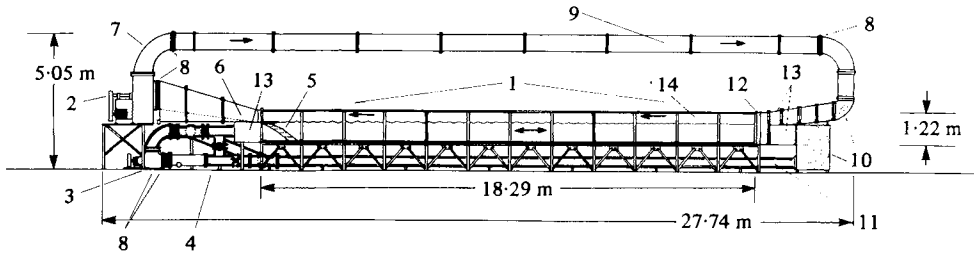


FIGURE 1. The wind, wave, and current interaction research facility at NASA Wallops Flight Center. (1) Test section, (2) suction fan, (3) 6000 GPM water pump, (4) valve assembly, (5) primary beach, (6) secondary beach, (7) fan discharge, (8) flexible joint, (9) air-flow duct, (10) flow turning vanes, (11) fibreglass piping (12), random-wave generator, (13) honeycomb section, and (14) plate-glass side.

system (type 1014 electronic manometer and type 572 ultra-high accuracy transducer) was used. Height *versus* velocity data were taken at a minimum of twelve points along each profile. Several minutes of averaging were done at each reading, proceeding from maximum to minimum height and then returning to the maximum along heights between those used in descending. The measured wind profile was used to calculate the frictional velocity,  $U_*$ , and the roughness length scale,  $Z_0$ , by employing the standard logarithmic profile formula

$$U(Z) = \frac{U_*}{\kappa} \ln \left( \frac{Z}{Z_0} \right), \quad (3.1)$$

where  $Z$  is the height above the mean water level and  $\kappa$  is the von Kármán constant. All combinations of two points along the wind profile, excluding the pairs of adjacent points, are used to solve  $U_*$  and  $Z_0$  in a Hewlett-Packard 9825A calculator. Thus many pairs of  $U_*$  and  $Z_0$  values are calculated. Typical standard deviation of the  $U_*$  and  $Z_0$  values were below 3% and 10% respectively.

Concurrently with the measurements of the wind profile, a Nicolet UA500A spectrum analyser was used to produce a frequency spectrum of the wave height. The height spectrum produced represents the average of 128 spectra of resolution of 0.1 Hz, with 256 degrees of freedom and a normalized statistical error of 8.84%. The spectrum was then transferred electronically through an interface into the main controlling device, a Hewlett-Packard 9825A, where other operations occur under program control. Here the spectrum was processed with proper calibration information. The results were stored on a digital cassette, and other products were developed from it, such as r.m.s. height and various theoretical calculations. The final plot of the spectrum was obtained from a Hewlett-Packard 9872A plotter, under control of the HP9825A, while the various calculated products appeared as a printout.

For each set of experimental conditions, a Nicolet UC202C correlator was used to produce seven independent measurements of the probability distribution of the surface elevation measured by the capacitance-type wire probe. Each of these seven probability distributions is based on 1.31 million data points, acquired with a sampling period of 0.1 ms. After completion of each distribution measurement, the probability distribution is transferred through a digital interface to a Hewlett-Packard 9825A. There it is normalized and the cumulants are calculated. A plot of the normalized distribution is then produced on a Hewlett-Packard 9872A plotter, under control of

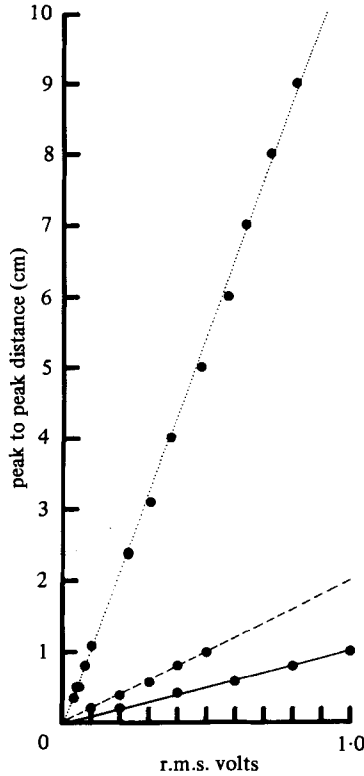


FIGURE 2. Calibration data for the wave measurements system. . . . ., 11.2 cm peak to peak; - - -, 1.96 cm peak to peak; —, 1.01 cm peak to peak.

the 9825A. When all seven distributions are thus processed, the mean probability distribution and the mean of each cumulant up to the eighth cumulant is produced, along with the standard deviations from each mean, respectively. Using the mean cumulants thus produced and calculating the appropriate Hermite polynomials, the Gram-Charlier series is then computed, checked for normalization, and plotted in comparison with the mean probability distribution.

From the wave-height spectrum, the frequency of the spectrum peak,  $n_0$ , is determined, and the equation

$$n_0^2 = gk_0 + \gamma k_0^3, \tag{3.2}$$

is solved for wavenumber  $k_0$ , where  $g$  is the gravitational acceleration, and  $\gamma$  is the surface tension. Notice that here  $n_0$  is in radians  $s^{-1}$ . The wavelength,  $\lambda_0$ , corresponding to the peak frequency,  $n_0$ , is then known and used with the r.m.s. wave height,  $(\zeta^2)^{\frac{1}{2}}$  to calculate the significant slope,  $\xi$ .

The whole data-processing system was calibrated by oscillating the wave-height gauge at various known amplitudes and a fixed frequency of 1.8 Hz. The signal from the probe was processed as a single train of waves through the correlator. The measured r.m.s. values through the system were plotted against the known r.m.s. amplitudes as in figure 2. This figure demonstrates the linearity of the measurement system.

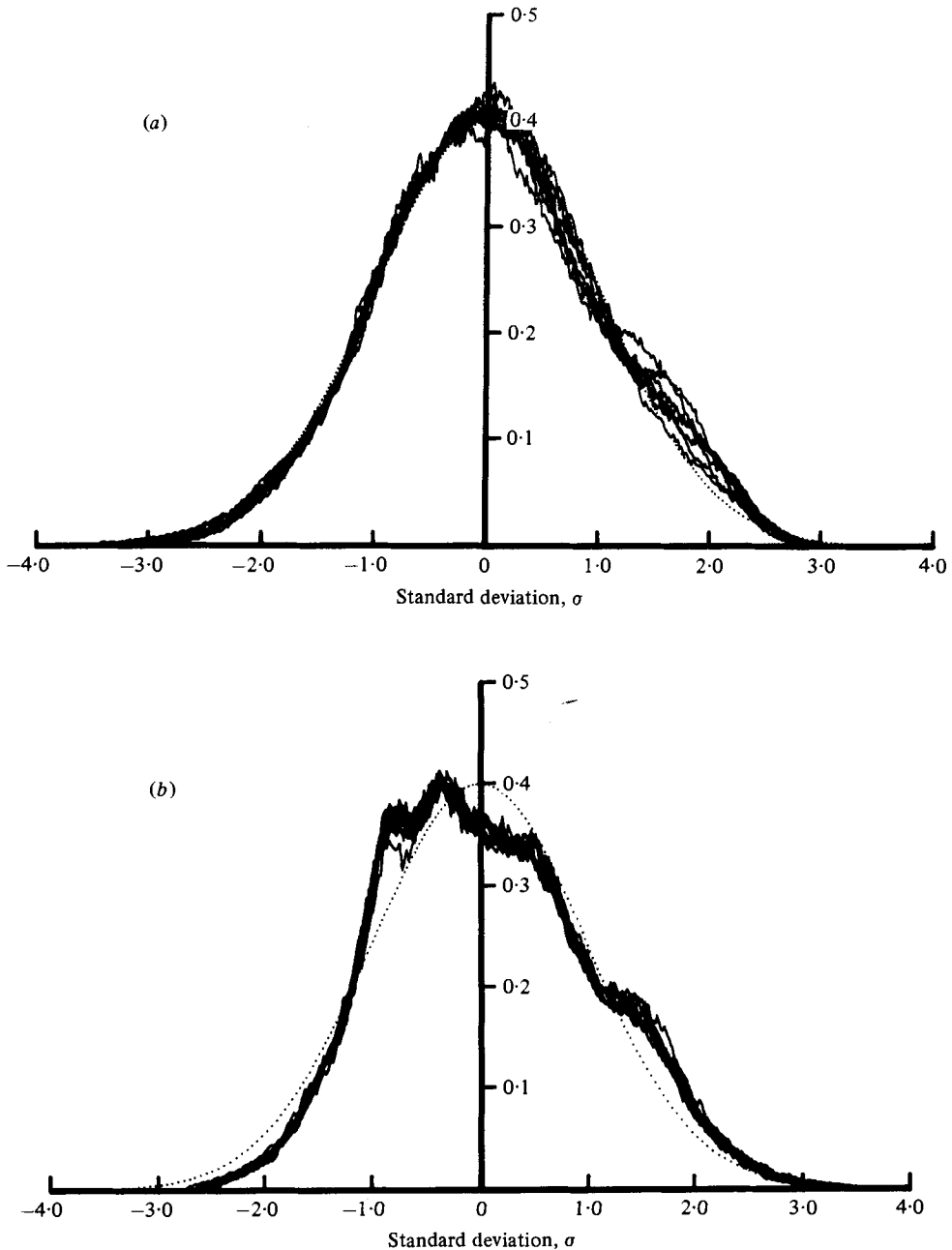


FIGURE 3. For legend see p. 186.

#### 4. Results

Typical measured probability distribution functions are shown in figure 3(a)–(f) in a sequence of increasing wind speed. As the wind speed increases, the distribution functions become increasingly skewed and eventually reach a value of unity. The changes of the skewness value of the distribution as a function of  $U_*/C_0$  with  $C_0$  as the phase velocity of the wave at the spectral peak is shown in figure 4. The dark circles in figure 4 indicate the cases with multiple secondary peaks on the measured

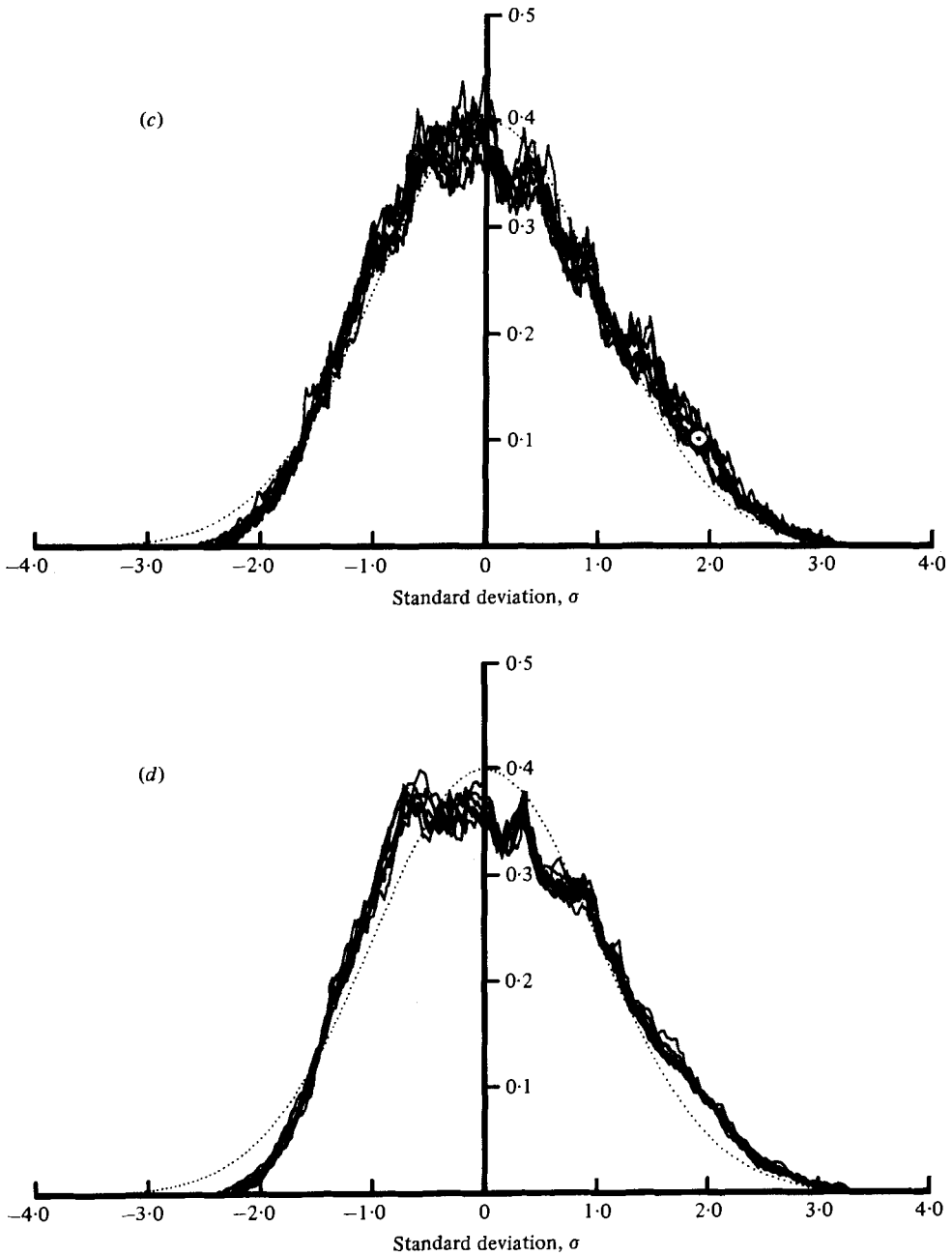


FIGURE 3. For legend see p. 186.

distribution function. Those cases generally occurred in the wind speed range of  $U_* = 23$  to  $35 \text{ cm s}^{-1}$  (or  $U_*/C = 0.7-0.9$ ). As the wind speed increases, the occurrence of the secondary peak becomes less frequent.

There is a particularly interesting phenomenon in the changes of skewness *versus*  $U_*/C_0$ ; that is the skewness may assume a negative value at low  $U_*/C_0$  values ( $U_*/C_0$  less than 0.6). All these cases are also under low wind speed ( $U_* < 17 \text{ cm s}^{-1}$ ). At such

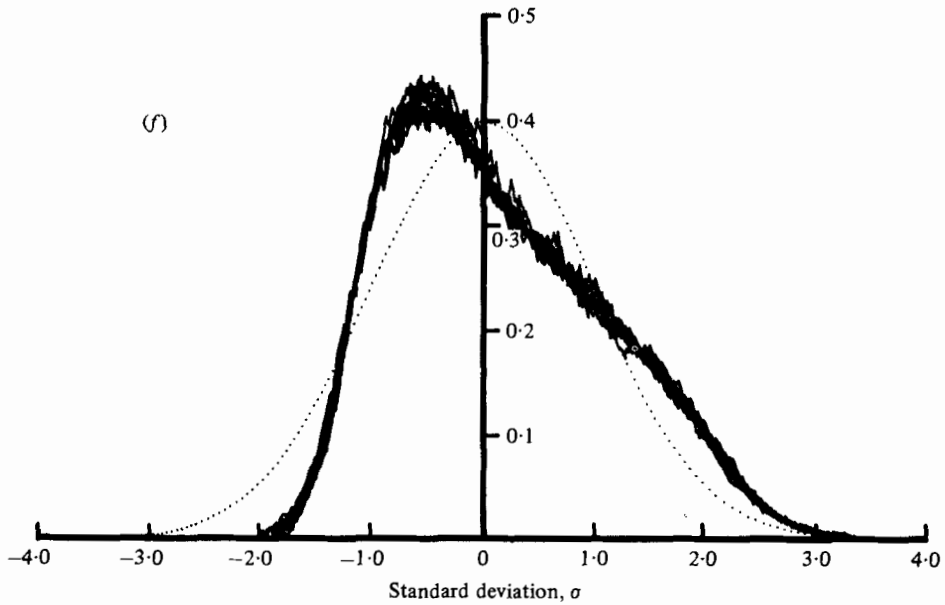
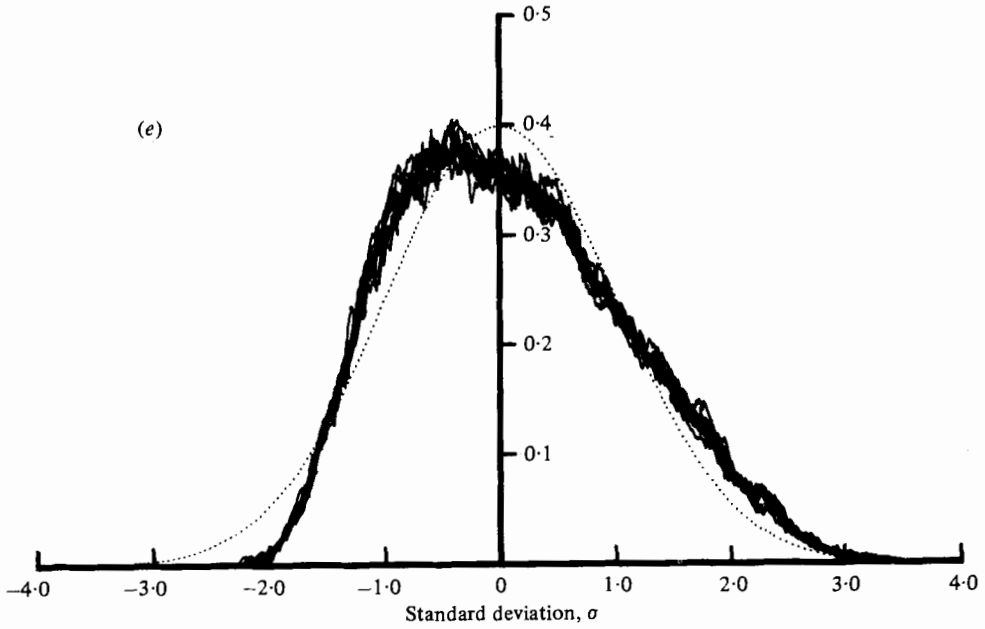


FIGURE 3. The normalized distribution of wave height for the cases listed in table 1. Each case represents seven independent measurements under the same conditions. , Data; , normalized Gaussian distribution.

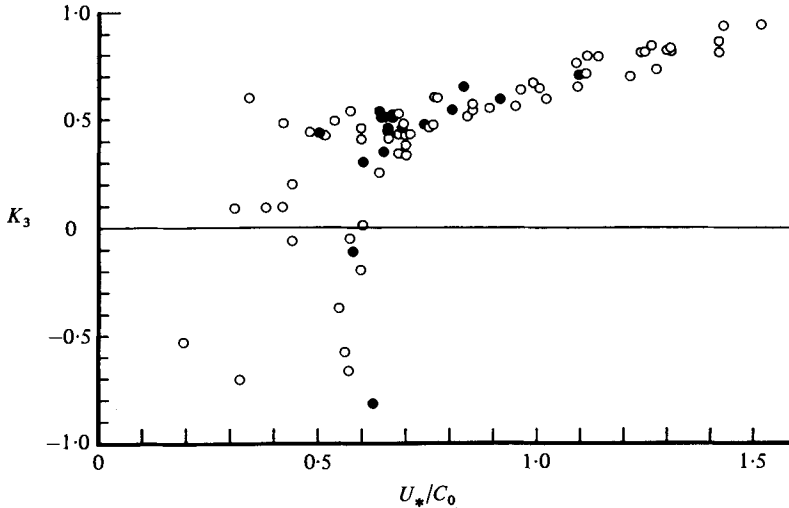


FIGURE 4. The variation of skewness,  $K_3$ , with  $U_*/C_0$ .  $C_0$  is the phase speed of the wave with frequency  $n_0$ , the frequency of the maximum in the wave-height frequency spectrum. The presence of secondary peaks and fine structure on the probability distribution is denoted by ●; no discernible fine structure is denoted by ○.

wind speed, the waves at the surface are just beginning to become visible. Those waves are predominately ripple-like, while their typical spectra exhibit multiple peaks in the capillary-gravity range. By the finite-amplitude wave theory in the capillary range developed by Crapper (1957), the profile of the wave may indeed become sharp troughed and round crested. Thus the negative skewness becomes intelligible. However, since only a contact probe was used in this study, the accuracy in the capillary range is really doubtful. This may explain the wide scattering of the data points in this range. Because of this uncertainty, all the points with  $U_*/C_0 < 0.6$  will not be included in this discussion.

As the wind increases, beyond  $U_* = 17 \text{ cm s}^{-1}$ , the wave spectrum begins to assume a more definite single predominant peak form and its skewness stays positive all the time. At high wind cases when the skewness approaches 1, a gentle hump appears on the positive side of the distribution curve as shown in figure 5. This hump indicates an excess of occurrence frequency at that particular height. If a smooth curve is fitted through the distribution, one finds the humps are, in general, centred around  $1.4(\zeta^2)^{\frac{1}{2}}$ , which is precisely the location of the mean amplitude of the waves. This hump is an indication that the amplitudes of the waves have a preferred range of height rather than appearing completely random. This is also consistent with the fact that the spectra of even the wind-generated random waves are rather narrow-peaked. Other than these general observations, two specific analyses are summarized as follows.

(a) *The higher-order cumulants*

If the surface elevation distribution is exactly Gaussian, then all cumulants with order higher than two should be zero. However, owing to the nonlinear effects, the true distribution of the surface elevation is no longer Gaussian as indicated by the

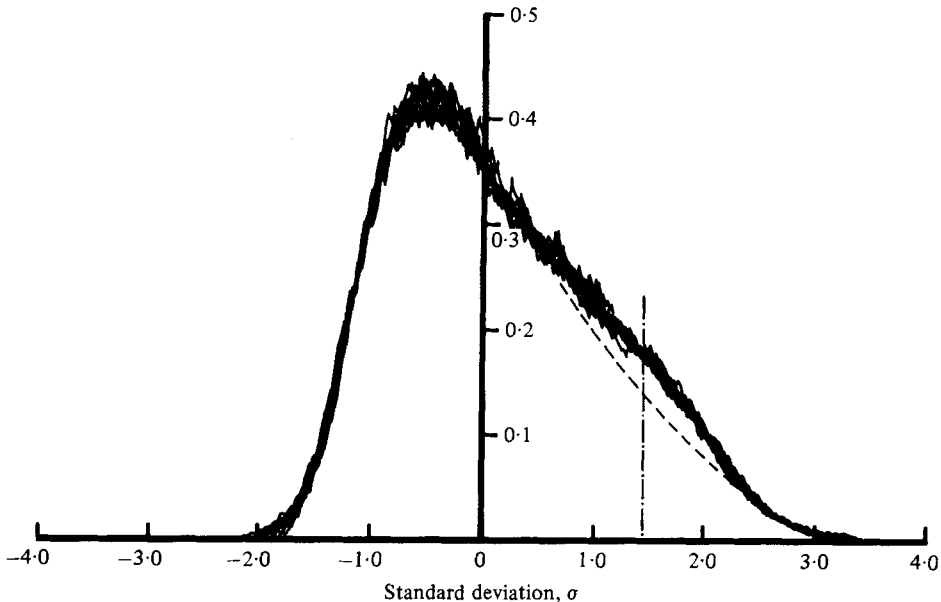


FIGURE 5. The normalized distribution of wave height for case (*f*) of table 1. Note the increase in the distribution about  $2\frac{1}{2}\sigma$ , marked by - - - - -.

sharp peaks and rounded troughs of the waves. This distortion is due to the energy in the higher harmonics. If so, the magnitude of this distortion should be proportional to the steepness of the energy-containing waves, which is measured by the significant slope,  $\xi$ .

Of particular interest is the skewness. The results of the laboratory data, limited field and satellite data are given in figure 6. Limited field data from Kinsman (1960) were also plotted. Since the significant slopes in the field are in general lower, the skewness is also less. Although considerable scatter exists in Kinsman's data, the majority of the data points and the mean value do fall within the theoretically established limits as discussed earlier by Longuet-Higgins (1963). It should be pointed out that, although Kinsman (1960) claimed that the distribution would approach to Gaussian as the wind speed or amplitude of the waves increases, such a trend was not detected clearly in the data. In fact, theory and laboratory data indicated the contrary.

A third source of data, also from the field, is derived from a satellite altimeter. A detailed discussion of the applications of the altimeter can be found in McGoogan (1974) and Walsh (1979). Briefly, an altimeter is a simple pulsed radar for distance measurement. However, if the pulse sent by the radar hits the sea surface, the returned pulse shape contains the statistical information of the sea surface height distribution (Walsh 1979). From the two cases studied by Walsh using GEOS-3 data, two additional points are plotted in figure 6. The skewness of these points is derived from the returned pulse shape, while the  $\xi$  values are based on the ground truth data from surface buoys. The values again agree well with both the mean field data and the laboratory data. A best-fitted curve through all the laboratory data, the mean of the *in situ* field data, and the remotely sensed data gives

$$K_3 = 8\pi\xi. \quad (4.1)$$

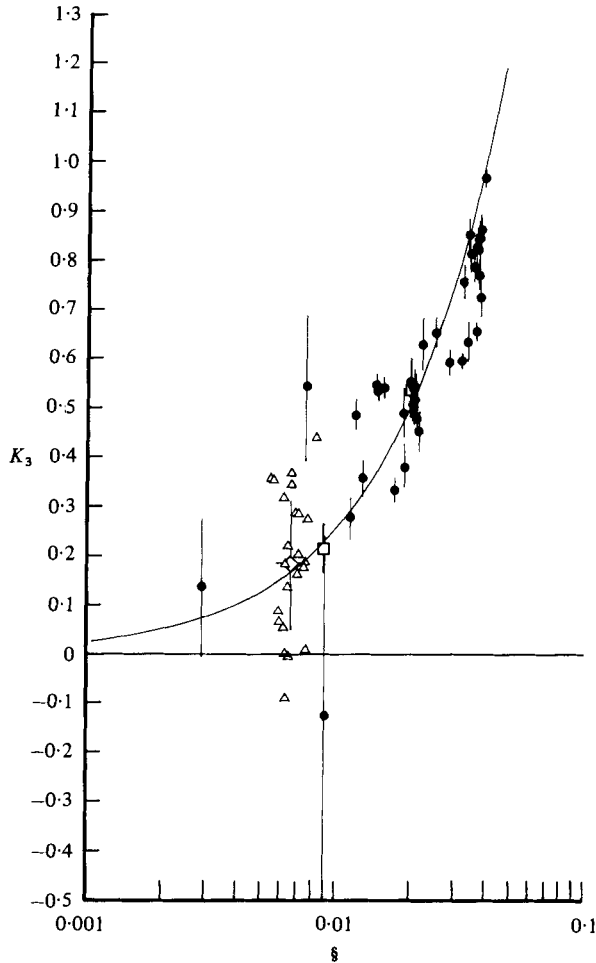


FIGURE 6. The variation of skewness,  $K_3$ , with significant slope,  $\S$ . ●, Data of the present study, with one-sigma error bars;  $\triangle$ , results of Kinsman (1960);  $\diamond$ , average of Kinsman's (1960) results with one-sigma error bars;  $\square$ , remotely sensed data of Walsh (1979) with one-sigma error bars. The best-fitted curve,  $K_3 = 87\S$ , is shown by the solid line.

Starting from a very general set of assumptions, Longuet-Higgins (1963) showed that the skewness of the distribution of surface elevation could be expressed in terms of the directional energy spectrum. But for lack of a definitive theoretical form of the directional spectrum no attempts were made to derive the possible theoretical form of  $K_3$ . It suffices here to say that the trend of variation of  $K_3$  is proportional to the slope of the waves as suggested by Phillips (1961).

As a further measurement of the deviation of the surface elevation distribution from the Gaussian, the normalized higher-order cumulants of the laboratory data are calculated up to the 8th order, as shown in figures 7(a)–(e) and in table 1, where six representative cases are given.

The data on the higher-order cumulants are highly coherent and self-consistent. The standard deviation of each seven independent measurements under the same

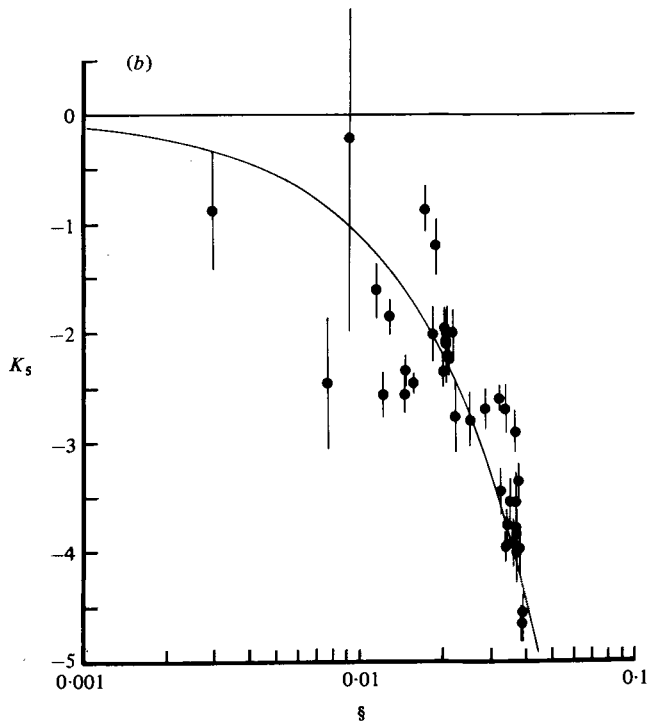
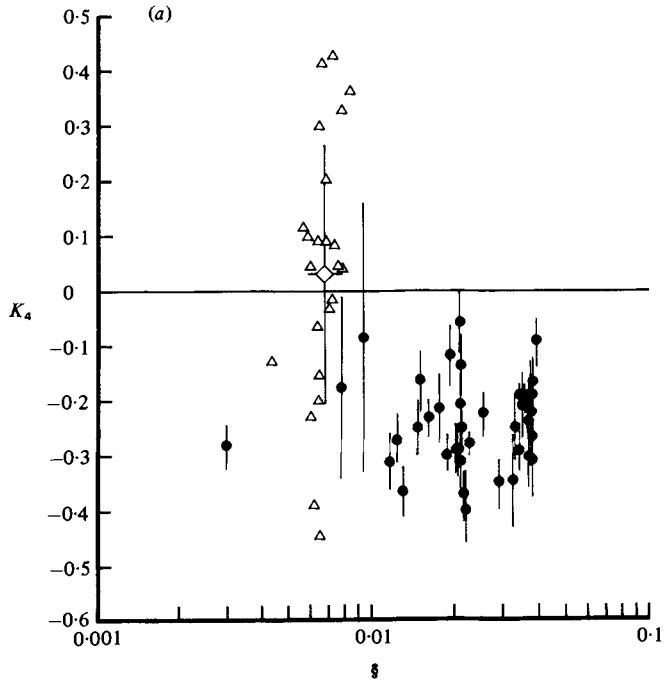


FIGURE 7. For legend see p. 192.

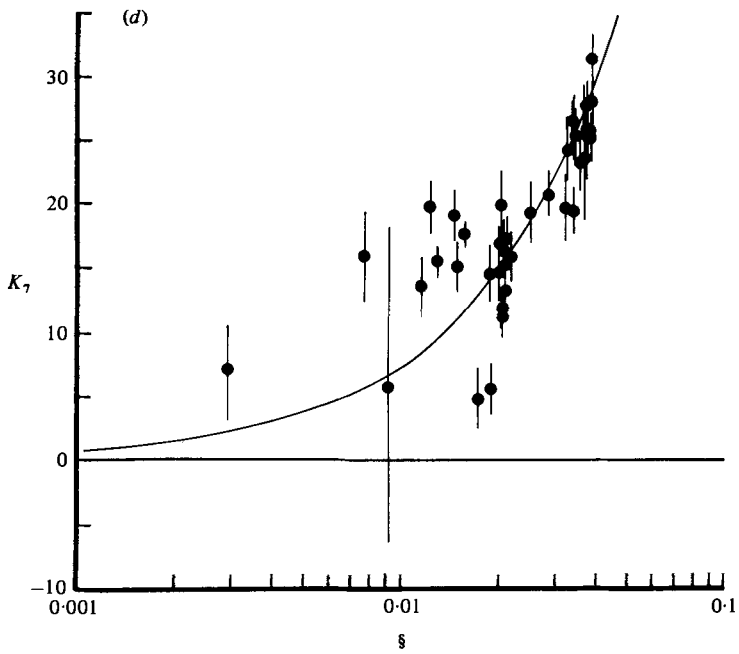
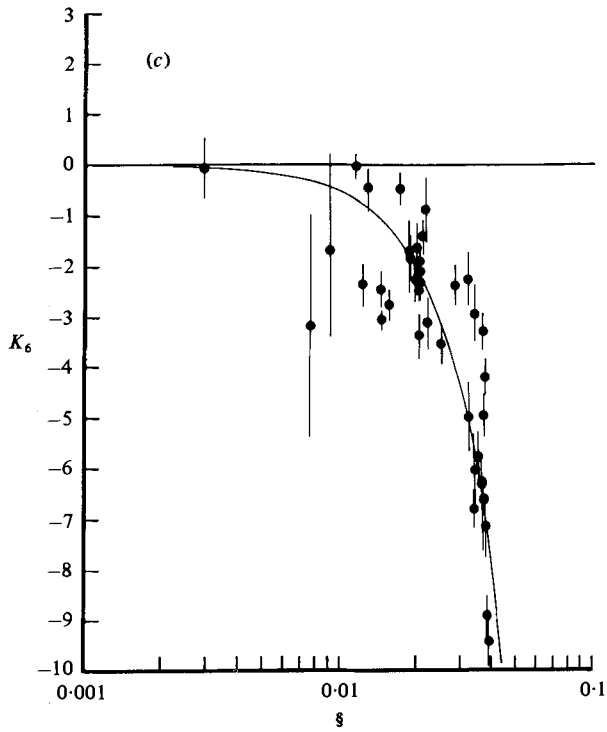


FIGURE 7. For legend see p. 192.

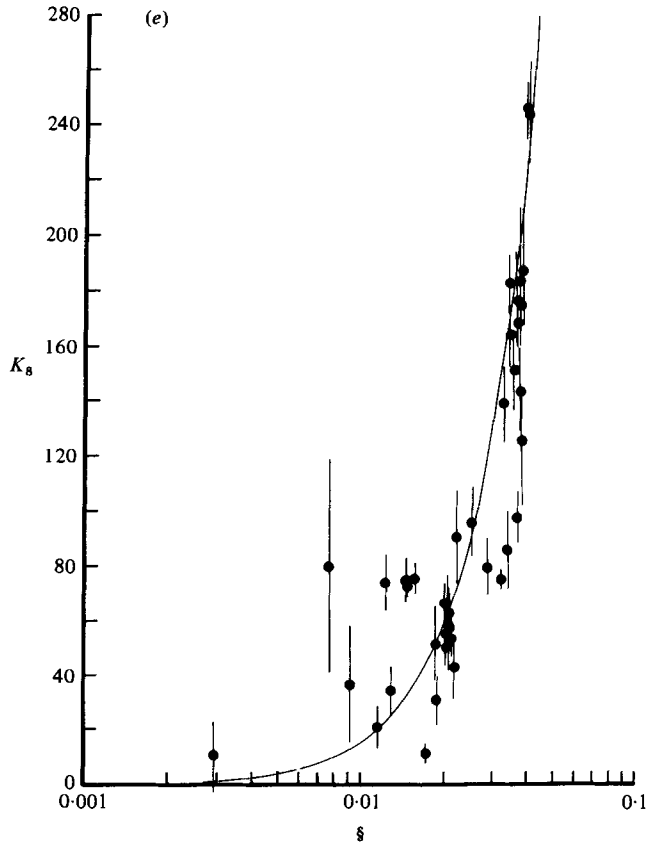


FIGURE 7. The variation with significant slope,  $\xi$ , of the higher-order cumulants: (a) flatness,  $K_4$ , using the symbols of figure 6; (b)  $K_5$ , including the line given by (4.2); (c)  $K_6$ , including the line given by (4.3); (d)  $K_7$ , including the line given by (4.4); (e)  $K_8$ , including the line given by (4.5).

condition is shown by the error bars in the figures. They are typically less than 10%. The trend of the value changes is also coherent. The self-consistency, coherence and high degree of repeatability of all the data from the laboratory and field in the trend can be used as an indication of the fact that the trend could be regarded as genuine. As we can see, all cumulants other than  $K_4$  show a clear trend as a function of  $\xi$ .

The flatness data,  $K_4$ , are quite scattered. No clear trend can be detected, but the values are largely confined within the range of  $-0.1$  to  $-0.4$ . This lack of coherent pattern lacks proper explanation. When higher cumulants are calculated, trends again become visible;  $K_5$  and  $K_6$  are generally negative. The maximum value of  $K_5$  reaches the neighbourhood of  $-5$ , while  $K_6$  reaches  $-10$ ;  $K_7$  and  $K_8$  are all positive. The maximum value of  $K_7$  reaches 30,  $K_8$  reaches 250. By curve fitting of the data, we found that all higher-order cumulants change rather regularly as function of the significant slope. The empirical forms are

$$K_5 = -110\xi, \quad (4.2)$$

$$K_6 = -5000\xi^2, \quad (4.3)$$

Case	$U_*$ (cm s <sup>-2</sup> )	$(\overline{\xi^2})^{\frac{1}{2}}$ (cm)	$K_3$	$K_4$	$K_5$	$K_6$	$K_7$	$K_8$
(a)	12.22	0.0353	0.2031	-0.2021	-1.3612	-0.7015	10.0137	22.8891
Standard deviation	± 1.56	± 0.0013	± 0.0999	± 0.1057	± 0.4566	± 0.3427	± 4.0220	± 10.9765
(b)	20.32	0.0770	0.5461	-0.2540	-2.5476	-2.4269	19.1086	74.5107
Standard deviation	± 1.75	± 0.0019	± 0.0217	± 0.0535	± 0.1681	± 0.3783	± 1.9887	± 8.0488
(c)	27.16	0.2225	0.4789	-0.3712	-2.2006	-1.3899	17.2866	53.5677
Standard deviation	± 2.76	± 0.0054	± 0.0264	± 0.0447	± 0.1675	± 0.3501	± 1.7316	± 7.4988
(d)	33.01	0.2988	0.5931	-0.3526	-2.6810	-2.3397	20.8897	79.2800
Standard deviation	± 2.59	± 0.0057	± 0.0268	± 0.0442	± 0.1843	± 0.4104	± 1.8463	± 9.9765
(e)	50.47	0.5660	0.6563	-0.3033	-2.8909	-3.2828	21.2226	97.4664
Standard deviation	± 7.44	± 0.0173	± 0.0176	± 0.0561	± 0.1886	± 0.3802	± 2.4530	± 9.4336
(f)	123.84	1.8777	0.9566	-0.1604	-4.6623	-8.8995	31.5235	246.1199
Standard deviation	± 13.70	± 0.0442	± 0.0166	± 0.0410	± 0.1414	± 0.3965	± 1.9675	± 11.0860

TABLE 1

$$K_7 = 750\$, \tag{4.4}$$

$$K_8 = 150000\$,^2. \tag{4.5}$$

The magnitude of the higher cumulants are presented in figure 7. The lack of scatter in each individual test and all the tests as a group seems to indicate that the sampling fluctuations is not a problem. However, this rapid increase in the values of higher-order cumulants certainly indicate some peculiar problems. For lack of definite theoretical forms for the higher cumulants, it is impossible to assess the cause of this trend of rapidly increasing values. This will undoubtedly cause trouble in the convergence of the characteristic function expansion and the Gram-Charlier approximation to be discussed next.

(b) Gram-Charlier approximation

The measured wave height distribution functions and their higher cumulants were used in the Gram-Charlier series as outlined in § 2. Since this series is an asymptotic expansion, the accuracy must be discussed. There are two principal causes of difficulties in the asymptotic approximation scheme. The first is the existence of all the higher cumulants which was discussed in the previous section. The second is the convergence of the expansions.

Theoretically, the series expansion given in (2.7) should be convergent for all values of cumulants. This might require a large number of terms which is unpractical if not impossible. To test the accuracy of a limited number of terms for the Edgeworth expansion, one high-wind case is chosen as an example for detailed study. The mean probability distribution function has been fitted with Edgeworth's form as given in (2.7), starting from the normal, and then progressing up to the eighth term expansion. The results are shown in figures 9(a)-(c). Figure 9(a) gives the result of the Edgeworth

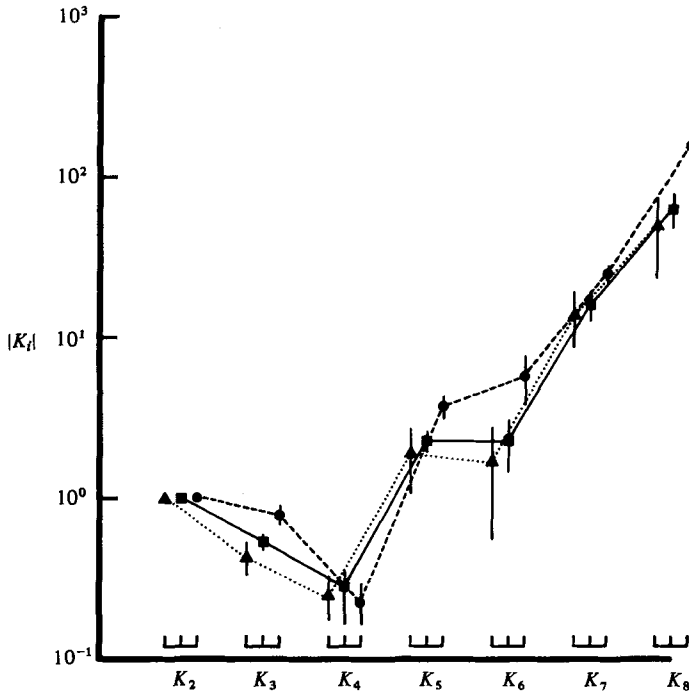


FIGURE 8. The relative magnitudes of the cumulants,  $|K_i|$ , for values of significant slope,  $\xi$ , of:  $\blacktriangle$ ,  $0.01 < \xi < 0.02$ ;  $\blacksquare$ ,  $0.02 < \xi < 0.03$ ;  $\bullet$ ,  $0.03 < \xi < 0.04$ . These three divisions are offset for clarity at each  $K_i$ .

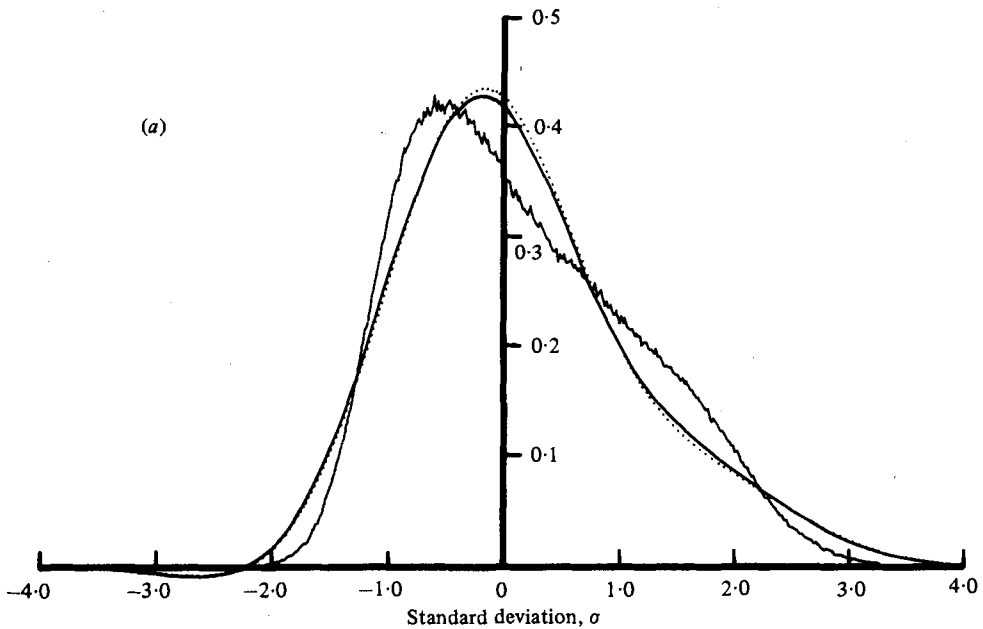


FIGURE 9 (a). For legend see facing page.

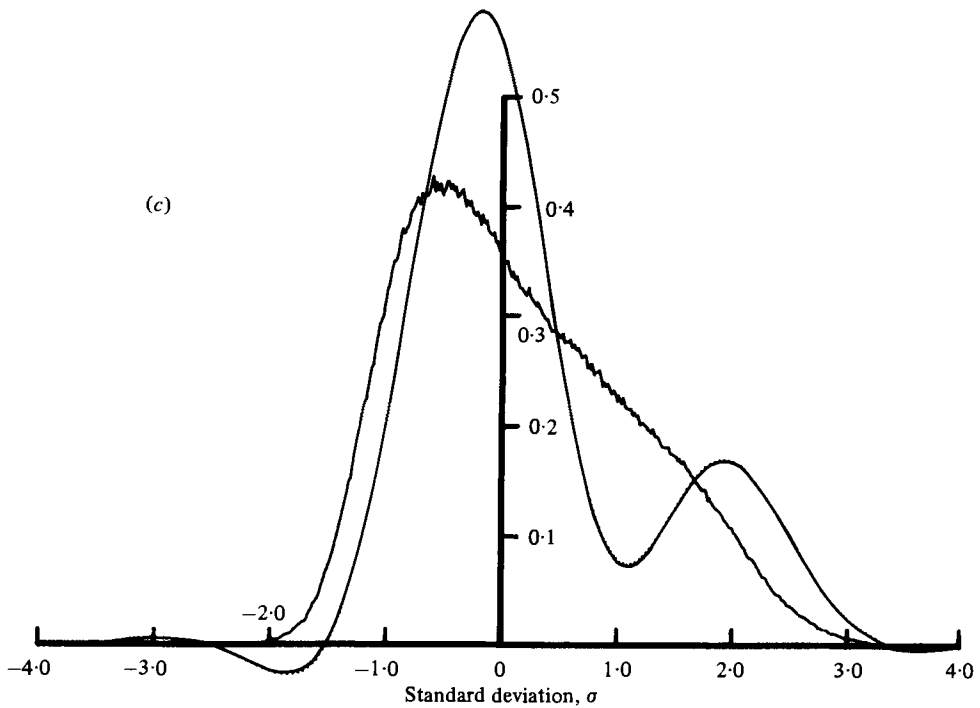
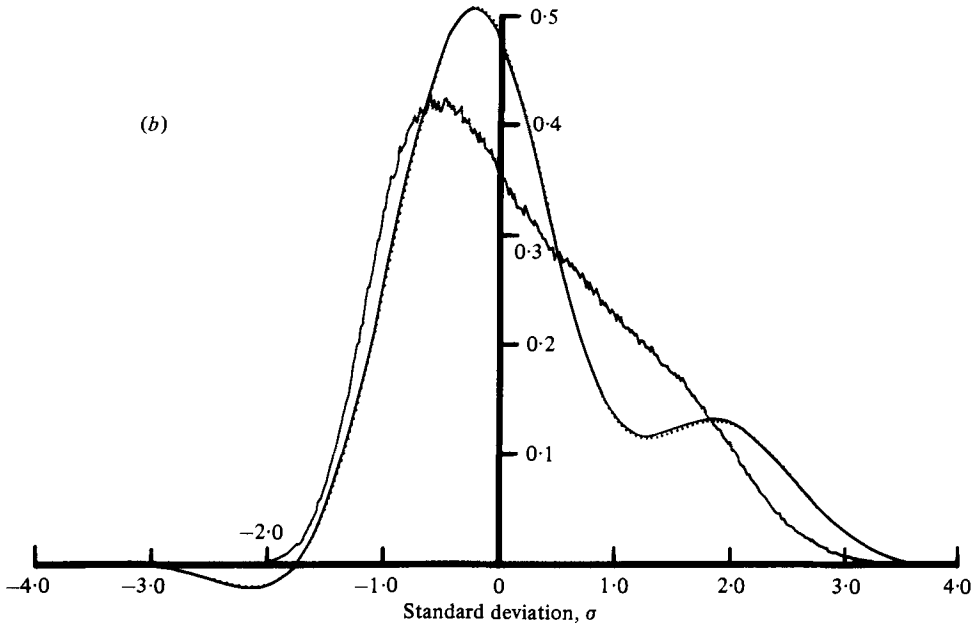


FIGURE 9. Using the distribution of wave height for case (f) of table 1, the Edgeworth form is fitted with an increasing number of terms stopping at the following  $H_i$ . (a)  $\dots$ ,  $H_3$ ,  $\text{---}$ ,  $H_4$ . (b)  $\dots$ ,  $H_5$ ;  $\text{---}$ ,  $H_6$ . (c)  $\text{---}$ ,  $H_7$ ;  $\dots$ ,  $H_8$ . Here  $H_i$  are the Hermite polynomials. Note the worsening of the fit for an increasing number of terms.

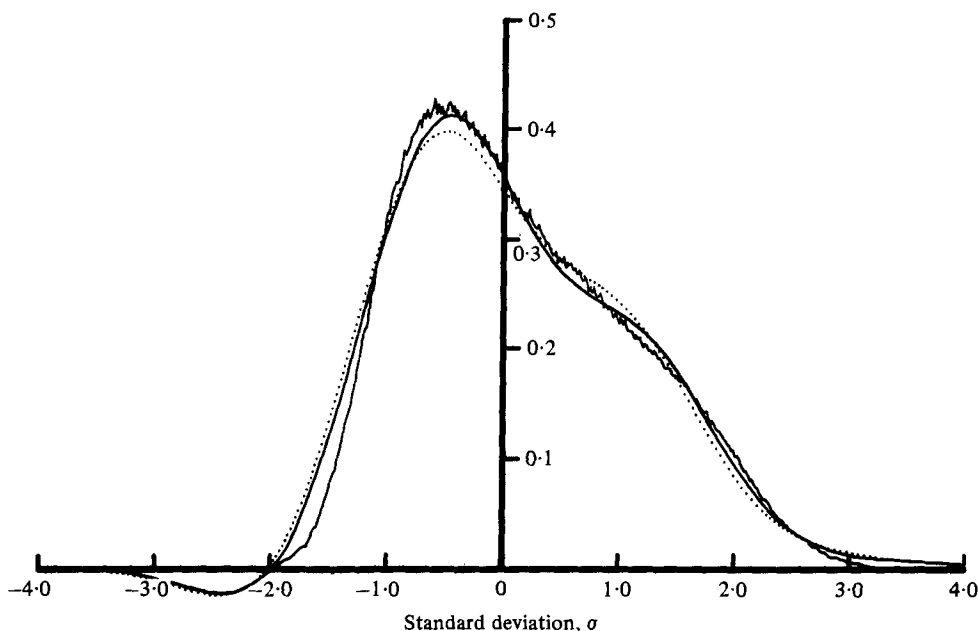


FIGURE 10. Using the distribution of case (f) of table 1, the expansion suggested by Longuet-Higgins (1963), given by (2.10), appears as —; the eight-term Edgeworth form, limited by  $K_i \leq 4$ , appears as . . . . .

form up to  $K_3$  and  $K_4$ . As higher-order terms are included, the Edgeworth form yields results less satisfying. Figure 9(b) gives the result up to  $K_5$  and  $K_6$ , while figure 9(c) represents the highest orders attempted,  $K_7$  and  $K_8$ . From these figures, it is clear that the approximation does not improve, but actually deteriorates, as more and more terms are included. The uniformly poor results of all the approximations seems to confirm that either the higher-order moments are indeed unreliable or the expansion given in (2.7) is not convergent uniformly. However it is well known that, even for a divergent asymptotic series expansion, an optimum number of terms can still give a good approximation (see, for example, Van Dyke 1975, § 3.5). We will try to see if such an optimization scheme exists or not. If it does exist, we could at least get a good distribution in spite of the uncertainties in the higher cumulants. The choice of the optimum number of terms is rather simple by using figure 8. The optimum number should be where the values of  $|K_i|$  reach a minimum. Using this criteria,  $K_4$  was chosen as the highest cumulant to be included. Thus the deterioration of the fitting by including more terms is understandable.

If we now consider the expansion given by Longuet-Higgins (1963), as in (2.10), the result of this fit is given in figure 10. Also appearing in figure 10 is a modified version of the Longuet-Higgins expansion. This consists of the eight-term Edgeworth expression, limited by  $K_i \leq 4$ , which is essentially the Longuet-Higgins form plus terms including  $K_4^2$  and  $H_8$ . The difference is small but the approximation deteriorates slightly for this case too. Judging from these comparisons, we concluded that the four-term modified Gram-Charlier expansion as suggested by Longuet-Higgins (1963)

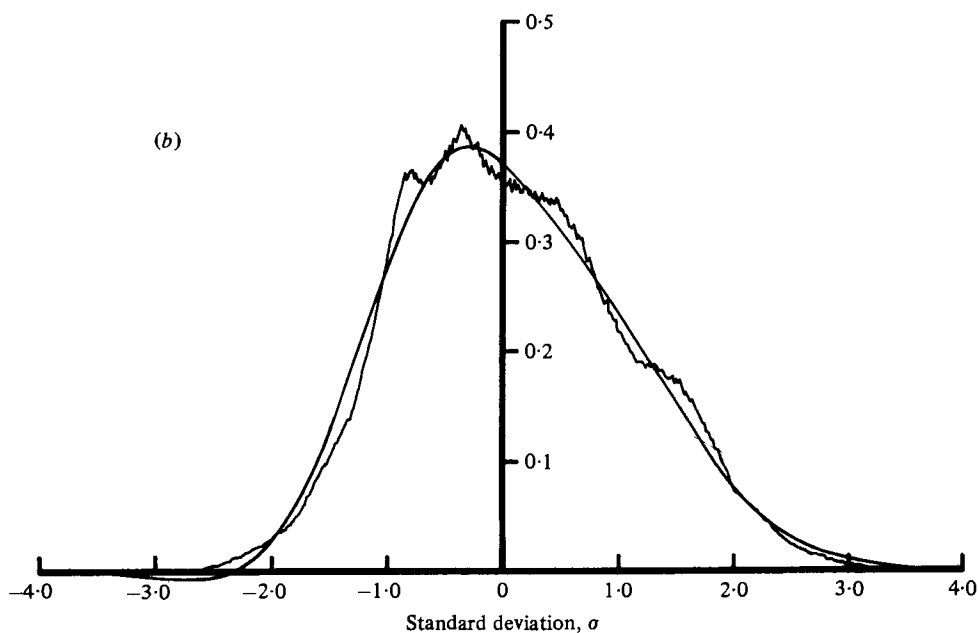
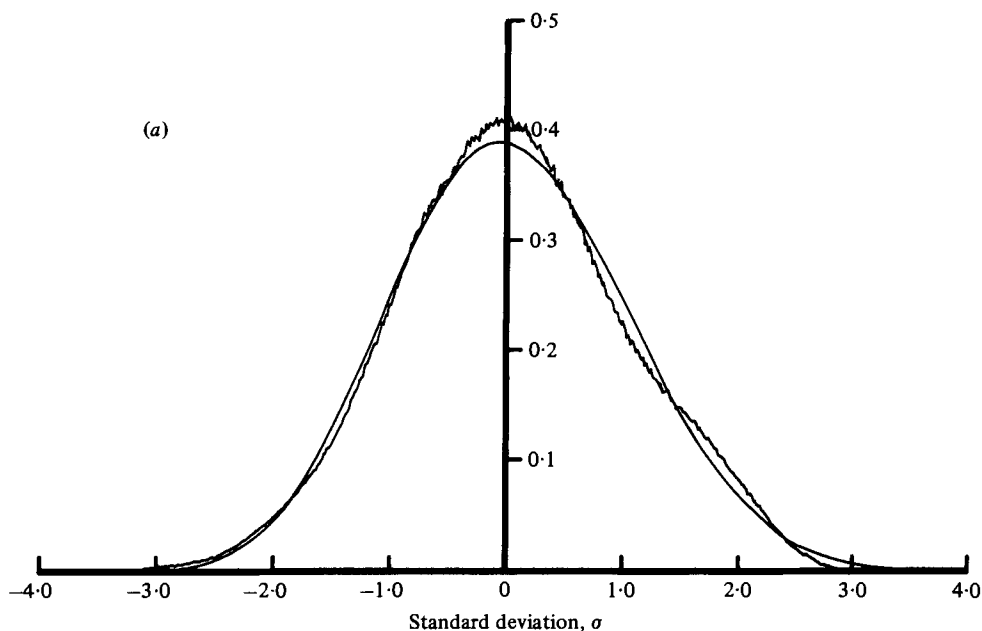


FIGURE 11. For legend see p. 199

gives the best approximation. Typical four-term Gram-Charlier fittings are given in figures 11(a)-(f), which represent the averaged distribution of figures 3(a)-(f) respectively.

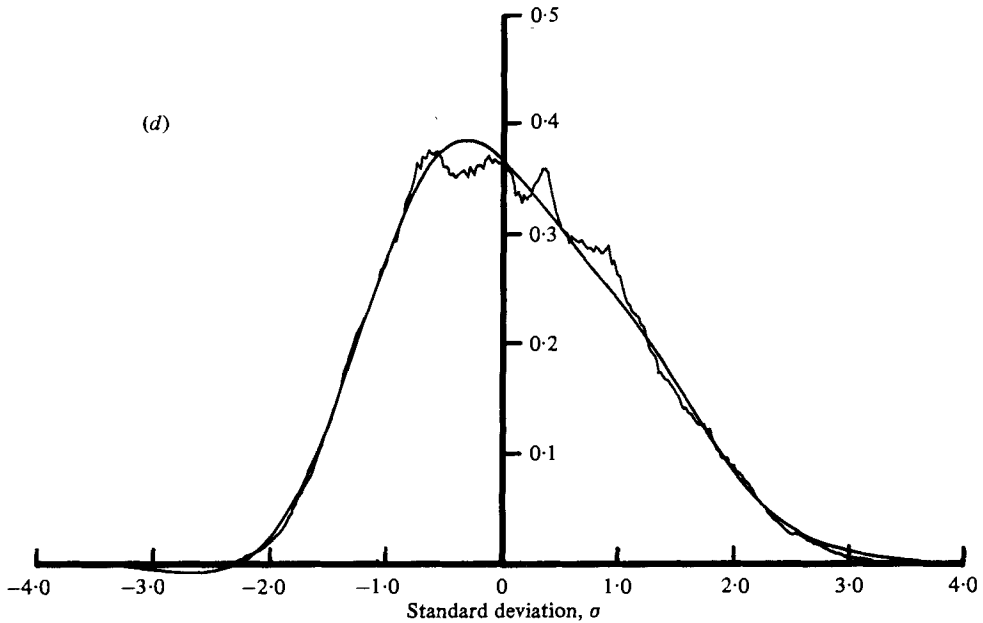
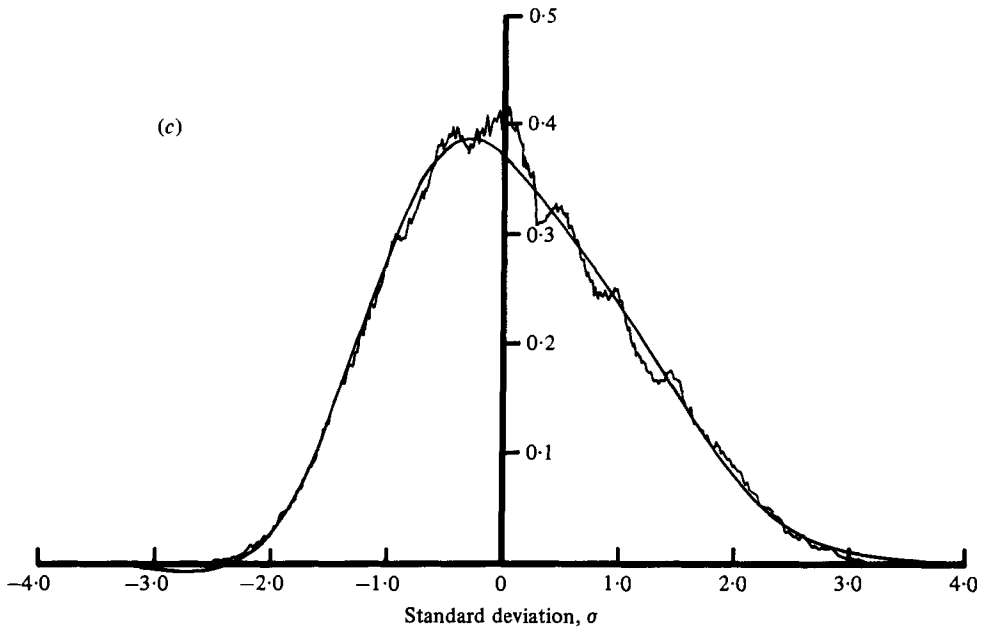


FIGURE 11. For legend see facing page.

## 5. Discussion and conclusion

The agreements between the theoretical results of Longuet-Higgins' (1963) study and our laboratory data, led us to conclude that the nonlinear analysis based on perturbation of potential motion of waves worked very well. There are some minor problems, however, that call for additional studies.

The first one is the slight negative value of the Gram-Charlier approximation at

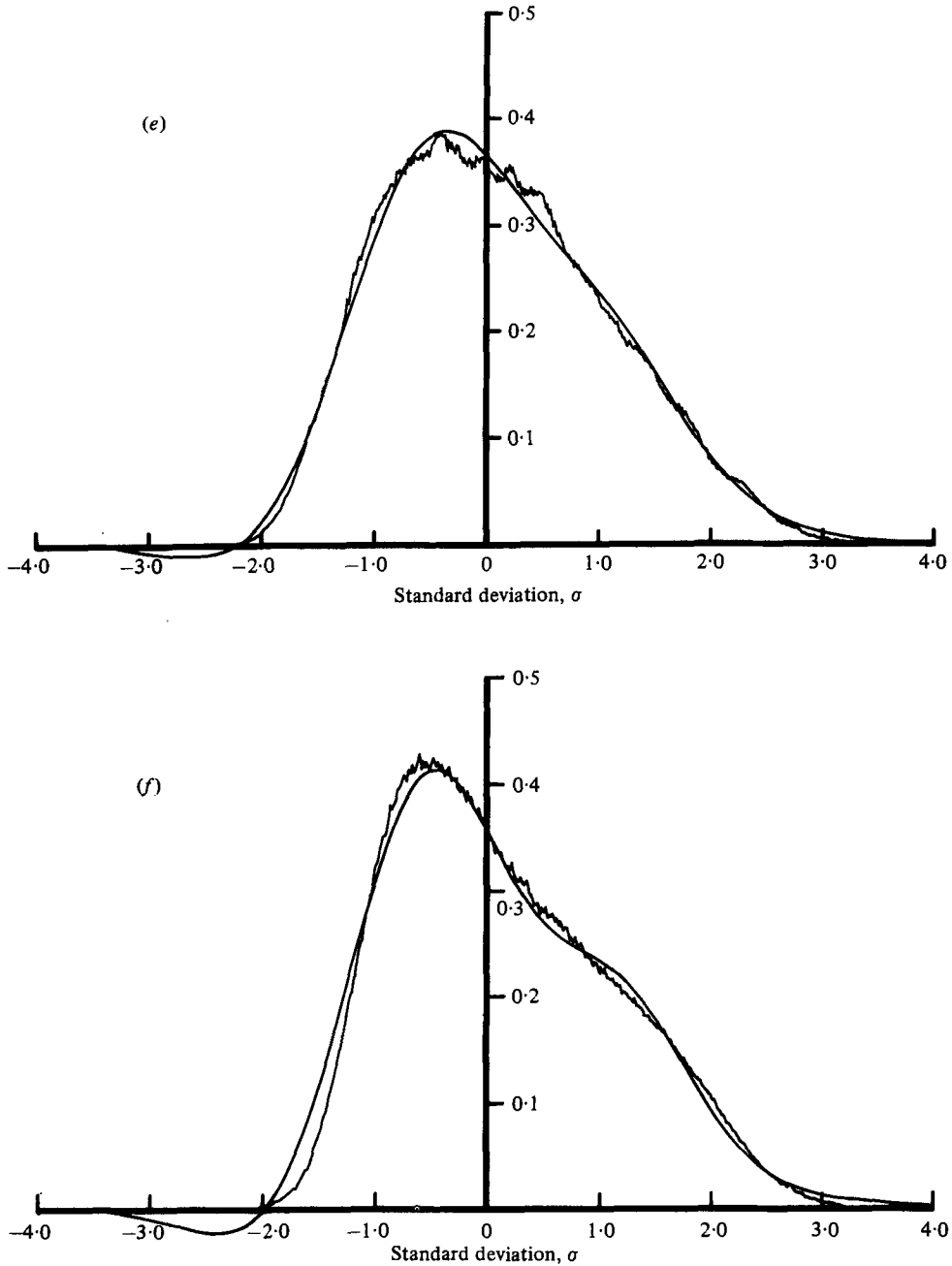


FIGURE 11. The expansion suggested by Longuet-Higgins (1963) used to fit the data of figure 3, for each case listed in table 1. The data now represents the average of seven independent measurements for each case of table 1 respectively.

large negative surface elevation, which is not meaningful. This negative value seems to be intrinsic in the expansion (see, for example, Kendall & Stuart 1963, § 6.20). It forces the final fitting to be biased negatively also. In our fittings using the four-

term approximation, the final results have been shifted slightly to balance the bias, under the requirement of a normalized distribution centred at  $\sigma = 0$ . The maximum shift caused by the negative tail is around 2%.

Secondly, there seems to be a tendency in the laboratory data for  $K_3$  to become negative for small  $\xi$  values. Interestingly, all the cases of negative  $K_3$  occur at extremely low  $\xi$  and wind speed ( $U_*/C_0 \leq 0.6$ ). At such wind speed the waves are just starting, and the peaks of the energy spectra are still in the gravity-capillary range. Those waves must have been generated by some instability mechanism (see, for example, Phillips 1977). The scatter of the data is considerably higher than the well-defined, higher  $\xi$  cases. Unfortunately, under the present laboratory set-up, we can only use wind to generate waves. The strong shearing stress in the laboratory is just not feasible for generating waves of gentle slopes. A definitive test has to wait until waves of gentle significant slope can be generated independently of the local wind by means of a paddle, say.

Finally, another area of future study is to derive theoretical expressions for higher-order cumulants similar to that of  $K_3$  of Longuet-Higgins (1963), considering the nonlinearity of the waves and the influence of the directionality of the wave propagation. Only by those theoretical results can one answer definitely whether the deterioration of the higher-order expansions is indeed due to sample fluctuations or series divergence. However, judging from the comparison of the four-term expansion with the data, any further improvement of the approximation to the probability distribution function will only be marginal.

The authors gratefully acknowledge the many helpful discussions and suggestions from Professor O. M. Phillips and Ms K. Burnett of the Johns Hopkins University, Professor C. C. Tung of North Carolina State University, Mr C. L. Parsons of NASA Wallops Flight Center and Dr L. F. Bliven of Oceanic Hydrodynamics, Inc. This work is supported by the N.A.S.A. Supporting Research Technology Program.

#### REFERENCES

- CRAMER, H. 1970 *Random Variables and Probability Distributions*, 3rd edn, cha. 4. Cambridge University Press.
- CRAPPER, G. D. 1957 An exact solution for progressive capillary waves of arbitrary amplitude. *J. Fluid Mech.* **2**, 532–540.
- KENDALL, M. G. & STUART, A. 1963 *The Advanced Theory of Statistics. Volume 1: Distribution Theory*, 2nd edn, §§3.12–3.15 and 6.20. London: Charles Griffin.
- KINSMAN, B. 1960 Surface waves at short fetches and low wind speed – a field study. *Chesapeake Bay Inst., Johns Hopkins Univ. Tech. Rep.* no. 19.
- LONGUET-HIGGINS, M. S. 1963 The effect of non-linearities on statistical distributions in the theory of sea waves. *J. Fluid Mech.* **17**, 459–480.
- MCGOOGAN, J. T. 1974 Precision satellite altimeter. *I.E.E.E. Intercon 74, Session 34(3)*, 1–7.
- PHILLIPS, O. M. 1961 On the dynamics of unsteady gravity waves of finite amplitude. Part 2. *J. Fluid Mech.* **11**, 143–155.
- PHILLIPS, O. M. 1977 *The Dynamics of the Upper Ocean*, 2nd edn. Cambridge University Press.
- VAN DYKE, M. 1975 *Perturbation Methods in Fluid Mechanics*, §3.5. Stanford, California: Parabolic.
- WALSH, E. J. 1979 Extraction of ocean wave height and dominant wavelength from GEOS-3 altimeter. *J. Geophys. Res.* **84**, 4003–4010.